Periodic Triangular Patterns in the Faraday Experiment

Hanns Walter Müller
Laboratoire de Physique, Ecole Normale Supérieure de Lyon, 46, Allée d'Italie, 69364 Lyon, France and Institut für Theoretische Physik, Universität des Saarlandes, D-66041 Saarbrücken, Germany
(Received 5 May 1993)

A pattern of standing surface waves in the form of equilateral triangles is observed in the Faraday experiment with two-frequency forcing. By perturbing with a third frequency the dynamics of a "phason mode" is under external control and transitions between triangles and hexagons can be enforced. The experiment is understood in terms of a three-mode amplitude equation model.

PACS numbers: 47.54.+r, 47.20.Ky, 47.20.Ma

The generation of standing surface waves on a fluid layer subjected to a vertical vibration (Faraday experiment [1]) provides a variable nonlinear pattern forming system. Depending on the geometry, the fluid parameters, and the excitation, spatially periodic structures in form of lines, squares, and hexagons have been observed [1–5]. Only recently the discovery of two-dimensional quasipatterns [3–5] (the macroscopic hydrodynamic analogy to quasicrystals in solid state physics [6]) has attracted much attention.

The present Letter reports the observation of a stable periodic pattern of equilateral triangles bifurcating supercritically from the basic state (plane surface). Even though investigated theoretically [7], periodic triangular structures have not yet been observed in experiments. Triangular and hexagonal patterns are closely related since both are composed of three plane waves, differing only by their relative spatial phases (see below). The mechanism selecting triangular patterns will be explained and contrasted to that mechanism which favors subcritically bifurcating hexagons in, e.g., non-Boussinesq convection [8]. On a more abstract level Golubitsky *et al.* [7] exhaustively discussed the bifurcation scenarios of triangular and hexagonal patterns by means of group theoretical tools. They carried out the discussion for Rayleigh-Bénard convection, but their arguments—based solely on the underlying symmetries—apply in a general context.

The experimental apparatus consists of a cylindrical plastic container of 80 mm inner diameter. To avoid meniscus waves, which might distort the determination of the stability threshold, the edge between the vertical sidewall and the bottom of the container is rounded by a curve of 1 cm radius thus reducing the diameter to 60 mm at the flat bottom. The dish is filled with 9 ml silicon oil Rhodorsil 47V20 giving a fill depth of about 2.3 mm. At 25 °C the fluid possesses a viscosity of 20×10^{-2} cm^2/s, a density of 0.95 g/cm^3, and a surface tension of 20.6×10^{-3} N/m. The container is mounted on the table of a vibration exciter, which accelerates periodically in the vertical direction according to

$$f(t) = a\,[r\cos 2\omega t + (1-r)\cos(4\omega t + \varphi)]\ , \qquad (1)$$

where $\omega = 2\pi \times 27.9$ Hz. The temperature of the fluid is measured by two thermistors in the bottom of the container and stabilized at 23 °C ± 0.1. During the experiment the overall acceleration amplitude a, relative amplitude r ($0 \le r \le 1$), and phase φ are continuously measured and controlled by a computer. As long as a is below a critical threshold $a_c(\omega, r, \varphi)$ the surface remains flat. To visualize the surface deformation the container is illuminated by a ring of inner/outer diameter 14/18 cm mounted 128 cm above the fluid. The light reflected at the surface is detected by a videocamera in the center of the ring. Further details of the apparatus are described elsewhere [5].

Figure 1 shows which standing surface pattern saturates if the forcing amplitude a is raised from a subcritical value to $\epsilon \equiv a/a_c - 1 \simeq 2\%$. Within the areas indexed by the subscript "s" the response of the system is subharmonic with respect to the total forcing frequency 2ω, i.e., the surface oscillates with ω and exhibits a wavelength $\lambda_s \simeq 0.72$ cm. Depending on r and φ either squares (S_s), hexagons (H_s), or triangles (T_s) appear. H_s and T_s have been combined in a common domain since a systematic separation is extremely time consuming and only partly

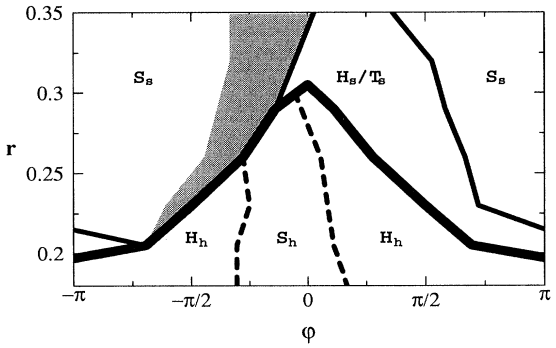

FIG. 1. Nonlinear stationary standing-wave patterns in the form of squares (S), hexagons (H), and triangles (T) saturate if the forcing amplitude $\epsilon = a/a_c - 1$ is raised from subcriticality to $\epsilon \sim 2\%$ above the primary instability of the flat surface. The subscript "s" ("h") denotes subharmonic (harmonic) response with frequency ω (2ω) and wavelength $\lambda_s \simeq 0.72$ cm ($\lambda_h \simeq 0.37$ cm). In the shaded domain slowly time-dependent disordered structures of length scale λ_s appear.

0031-9007/93/71(20)/3287(4)$06.00

possible: As soon as the forcing becomes supercritical the system randomly selects H_s or T_s on a (fast) time scale of $O(1/\epsilon)$. A subsequent very slow (phase dynamical) selection process finally decides between H_s and T_s, or else the pattern keeps fluctuating indifferently between the two structures. Figures 2(a)–2(c) presents photographs of the patterns as observed in the H_s/T_s region. To facilitate the identification we compare with computer generated density plots of ideal surface structures [Figs. 2(g)–2(i)] and the associated video images, which have been calculated by taking the (nonlinear) experimental visualization technique into account [Figs. 2(d)–2(f)]. The triangular pattern of Fig. 2(c) was stable during an operation time of several hours. Even though H_s have been reported earlier [3] this is the first time a stable periodic tesselation by equilateral triangles has been observed in a hydrodynamical experiment.

The thick black line in Fig. 1 marks the threshold of bicriticality separating the subharmonic region from the harmonic one. Below this line the $\cos(4\omega t)$ forcing is strong enough for the pattern to respond harmonically with respect to the total forcing period π/ω, i.e., to oscillate with 2ω and a wavelength $\lambda_h \simeq 0.37$ cm. Here, either squares (S_h) or hexagons (H_h) occur, while triangles never appear. Hexagons in harmonic resonance with the forcing have been observed earlier by Edwards and Fauve [4].

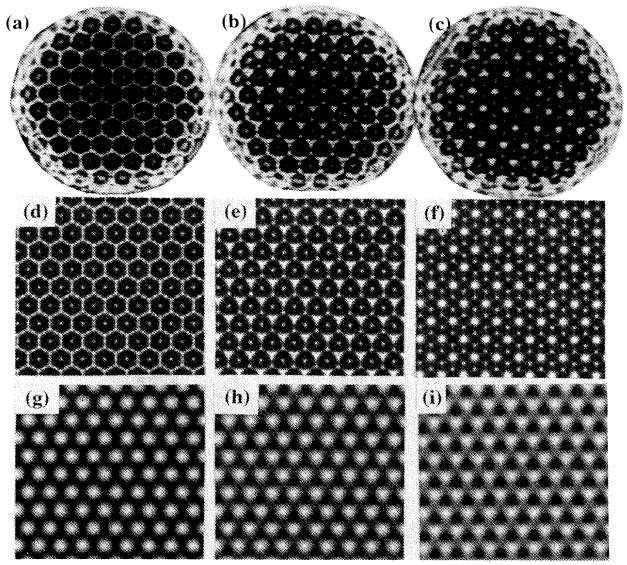

FIG. 2. Photographs (a)–(c) of nonlinear structures as observed in the T_s/H_s region of Fig. 1. For the sake of comparison computer-generated density plots are given for ideal surface patterns $\xi(x,y) = \cos(\mathbf{k}_1\cdot\mathbf{r})+\cos(\mathbf{k}_2\cdot\mathbf{r})+\cos(\mathbf{k}_3\cdot\mathbf{r}+\Phi)$, where $|\mathbf{k}_i| = k$ and $\mathbf{k}_1+\mathbf{k}_2+\mathbf{k}_3 = 0$. $\Phi = 0$ produces hexagons (g), $\Phi \simeq \pi/4$ triangles (h), and $\Phi = \pi/2$ regular triangles (i). The associated video images calculated by considering the experimental visualization technique are shown in (d)–(f).

Ignoring the influence of lateral boundary conditions the surface deformation in the form of N homogeneous superimposed standing waves can be expressed as [9,10]

$$\xi(x,y,t) = \left(\sum_{n=1}^{N} A_n e^{i\mathbf{k}_n\cdot\mathbf{r}} + \text{c.c.}\right) F(t) \ . \tag{2}$$

In the following we assume $|\mathbf{k}_n| = k_c$ and $\mathbf{k}_n \cdot \mathbf{k}_{n+1} = k_c^2 \cos(\pi/N)$ for $n = 1,\ldots,N$, i.e., the participating $\pm\mathbf{k}_n$ are equidistant on the circle of critical wave vectors. The real function $F(t)$ describes the temporal evolution of the response which is either harmonic or subharmonic. For the subharmonic case one has according to the Floquet theorem

$$F(t) = e^{i\omega t}\sum_l f_l e^{i2l\omega t} = \sum_l f_l e^{i(2l+1)\omega t} \ , \tag{3}$$

i.e., the subharmonic symmetry $F(t+\pi/\omega) = -F(t)$ is fulfilled, where π/ω is the total period of the forcing. The mode amplitudes A_n are supposed to vary slowly in time; they obey a set of coupled Landau equations which can be derived from the hydrodynamic equations by an expansion around the stability threshold. Without performing this derivation, the amplitude equations—up to cubic order—will have the form

$$\partial_t A_n = \epsilon A_n - \sum_{m=1}^{N} \beta(\theta_{mn})|A_m|^2 A_n \ , \tag{4}$$

where $\theta_{nm} = \angle(\mathbf{k}_n, \mathbf{k}_m)$. Even-order nonlinearities do not appear since the subharmonic symmetry of $F(t)$ enforces an $A_n \to -A_n$ invariance of Eq. (4). This temporal resonance condition is analogous to the Boussinesq symmetry in Rayleigh-Bénard convection.

Nonlinear pattern selection by Eq. (4) is governed by the coupling function $\beta(\theta)$, which depends—for a given experimental realization—on the forcing parameters r and φ. Spatial reflection and rotational symmetry imply $\beta(\theta) = \beta(-\theta) = \beta(\pi-\theta)$, while combinatorial arguments enforce $\beta(0) = \frac{1}{2}\beta(\theta \to 0)$ [11,12]. In the following we consider stationary solutions of Eq. (4) composed of equal amplitude plane waves, i.e., $A_n = Re^{i\phi_n}$ for $n = 1,\ldots,N$. ($N = 1$: lines; $N = 2$: squares; $N = 3$: hexagons or triangles; etc.) Then, that solution with the lowest corresponding free energy [12]

$$F_N = -\frac{\epsilon^2}{2}\left[\frac{1}{N}\sum_{m=0}^{N-1}\beta\left(m\frac{\pi}{N}\right)\right]^{-1} \tag{5}$$

is the most preferred structure. The other patterns are either metastable (less deep local minima of F) or unstable (local maxima of F). The dashed curve in Fig. 3 shows a typical coupling function favoring square structures [13] (since $F_2 \le F_N$ for all N). By slightly broadening the minimum of $\beta(\theta)$ one gets $F_3 \le F_N$ (solid line in Fig. 3) and patterns with $N = 3$ become the most stable ones.

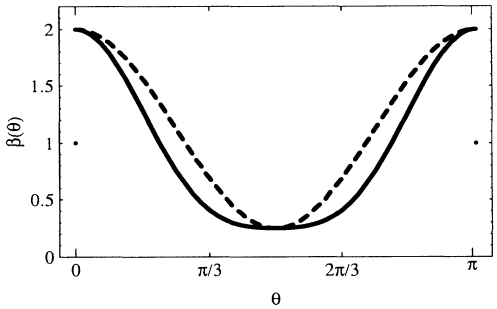

FIG. 3. Typical shape of a coupling function (dashed line) which minimizes the free energy (5) for square patterns, i.e., for $N = 2$. A slight broadening of the minimum (solid line) makes structures with $N = 3$ (hexagons or triangles) most stable. The functions $\beta(\theta)$ are discontinuous at $\theta = 0, \pi$. The curves $\beta(\theta) = 1/4 + 7/4\cos^2\theta$ (dashed) and $\beta(\theta) = 1/4 + 1/4\cos^2\theta + 3/2\cos^4\theta$ (solid) have been taken for demonstration purposes, and do not result from a strict derivation of Eq. (4).

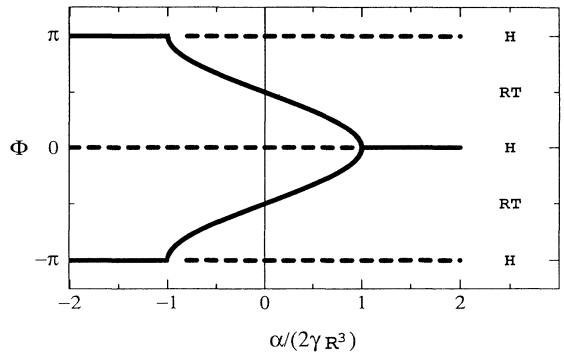

FIG. 4. Bifurcation and stability diagram for Φ resulting from Eq. (10) with $\gamma > 0$. The values $\Phi = 0, \pi$ ($\Phi = \pm\pi/2$) correspond to hexagons H (regular triangles RT), while intermediate values refer to triangular patterns (dashed=unstable, solid=stable).

This transition should occur in Fig. 1 at the border between the areas S_s and T_s/H_s.

The cubic mechanism in Eq. (4) with positive $\beta(\theta)$ saturates the mode amplitude R at $O(\epsilon^{1/2})$, but the phases ϕ_n remain degenerate: Introducing $A_n = Re^{i\phi_n}$ into Eq. (4) yields

$$\partial_t \phi_n = 0 \qquad \text{for} \quad n = 1, \ldots, N \ , \tag{6}$$

which gives N vanishing stability eigenvalues. Two of them are related to translations of the whole pattern in the horizontal directions while the remaining ones describe neutrally stable "phasons." In the case $N = 3$ (triangles/hexagons) this phason is conveniently parametrized by the (translationally invariant) combination

$$\Phi = \phi_1 + \phi_2 + \phi_3 \ . \tag{7}$$

By varying Φ the pattern changes continuously from hexagons ($\Phi = 0, \pi$) to regular triangles ($\Phi = \pi/2, 3\pi/2$) [see Figs. 2(g)–2(i)]. Structures with intermediate values of Φ are called triangles as opposed to regular triangles [7]. Generically the continuous symmetry degeneracy, which makes hexagons, triangles, and regular triangles equally stable, is lifted as soon as quintic contributions to Eq. (4) are considered [7]. Among the fifth-order terms compatible with the symmetries of the problem there is only one, $A_n^\star (A_{n+1}^\star)^2 (A_{n+2}^\star)^2$ (use $A_m^\star = A_{m-3}$ if $m > 3$), which affects the dynamics of Φ. Adding it (with a prefactor $-\gamma$, say) to the right-hand side of (4) leads to the phase equation

$$\partial_t \Phi = 3\gamma R^4 \sin(2\Phi) \ . \tag{8}$$

The fixed points of (8) are $\Phi = m\pi/2$ (m integer) corresponding to either hexagons (m even) or regular triangles (m odd). The former (latter) are stable if $\gamma < 0$ ($\gamma > 0$). Just above threshold the right-hand side of Eq. (8) is very small [$R^4 = O(\epsilon^2)$], in particular close to the hexagon-triangle transition, where $\gamma = \gamma(r, \varphi)$ goes through 0. This is the reason why the phason dynamics in the H_s/T_s region of Fig. 1 becomes extremely slow or even indifferent, rendering a systematic separation between the H_s and T_s domain impossible.

The cubic-quintic mechanism with positive $\beta(\theta)$ predicts supercritical bifurcations to S_s, H_s, and T_s. This is in accordance to the experiment, where all *subharmonic* bifurcations appear without a measurable hysteresis. The *harmonically* responding hexagons H_h, however, bifurcate slightly subcritically. Here, the responsible stabilization mechanism is more familiar: It is the same which generates hexagons by interacting quadratic and cubic nonlinearities in the amplitude equations (e.g., in non-Boussinesq convection). Since the harmonic symmetry does not impose a restricting resonance condition, even powers of A may appear in Eq. (4). Denoting by α the prefactor of a quadratic term in Eq. (4), the lowest order phase equation for the harmonic response reads

$$\partial_t \Phi = -3\alpha R \sin\Phi \ . \tag{9}$$

Equation (9) fixes Φ at either 0 or π, while stationary "triangular" solutions never exist. In the harmonic r-φ parameter region, where α goes through 0, the H_h pattern ceases to exist and supercritical S_h appear instead (between the dashed lines in Fig. 1).

The Faraday experiment with multifrequency forcing provides the possibility of operating the cubic-quintic and the quadratic-cubic stabilization mechanisms in the *subharmonic* regime. Then, the dynamics of Φ can be influenced externally and controlled transitions between triangles and hexagons are possible. To do so, we add a small perturbation $\mu\cos(\omega t + \psi)$ to the excitation (1), which generates even frequency contributions $e^{i2n\omega t}$ in

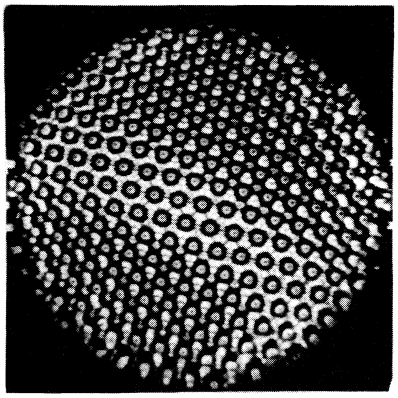

FIG. 5. Snapshot of a transient space dependent phason state. A wall of hexagons separates to areas of triangles. The picture has been taken from a cylindrical plastic container of 120 mm inner diameter with a mirror on the bottom to improve pattern visualization.

the response (3). Consequently, the subharmonic symmetry $F(t+\pi/\omega) = -F(t)$ is slightly broken and small even-order nonlinearities occur in (4). Neglecting quartic terms against quadratic ones the resulting phase equation becomes

$$\partial_t \Phi = 3R[\gamma R^3 \sin(2\Phi) - \alpha \sin \Phi] \ , \qquad (10)$$

where $\alpha = O(\mu)$. Figure 4 summarizes the bifurcation and stability behavior of the phase Φ, which turns out to depend on the parameter combination $\alpha/2\gamma R^3$. Starting from a stable regular T_s pattern (i.e., $\gamma > 0$) at $\mu = \alpha = 0$ one can continuously change to H_s by tuning α (via μ) or R (via ϵ). The patterns shown in Figs. 2(a)–2(c) (and any other for intermediate values of Φ) can be stabilized that way. More interesting phason dynamics can be achieved by changing periodically or randomly the sign of μ, or by modulating the phase ψ: As an example Fig. 5 shows a snapshot of a pattern with a transient space dependent phason state consisting of a H_s wall separating two areas of T_s.

The present Letter reports a hydrodynamic system, which exhibits a stable periodic pattern of equilateral triangles. Using symmetry arguments the experiment is explained in terms of a three-mode amplitude equation model. In contrast to the stabilization mechanism which involves quadratic terms (giving, e.g., weakly hysteretic hexagons in non-Boussinesq convection), the appearance of supercritical triangular patterns is associated with the interplay between cubic and quintic nonlinearities. By using both stabilization mechanisms simultaneously, controlled transitions between hexagons and triangles can be enforced.

I benefitted from discussions with W. S. Edwards, S. Fauve, K. Kumar, M. Lücke, and L. S. Tuckerman. This work is supported by Deutsche Forschungsgemeinschaft and Le Ministère Français des Affaires Etrangères.

[1] M. Faraday, Philos. Trans. R. Soc. London **52**, 319 (1831).
[2] S. Douady, J. Fluid Mech. **221**, 383 (1990).
[3] B. Christiansen, P. Alstrom, and M. T. Levinsen, Phys. Rev. Lett. **68**, 2157 (1992).
[4] W. S. Edwards and S. Fauve, C. R. Acad. Sci. Paris **315-II**, 417 (1992); Phys. Rev. E **47**, R788 (1993).
[5] W. S. Edwards and S. Fauve, "Patterns and Quasipatterns in the Faraday Experiment" (to be published).
[6] D. S. Shechtman, I. Blech, D. Gratias, and J. W. Cahn, Phys. Rev. Lett. **53**, 1951 (1984).
[7] M. Golubitsky, J. W. Swift, and E. Knobloch, Physica (Amsterdam) **10D**, 249 (1984).
[8] E. Palm, J. Fluid Mech. **8**, 183 (1960).
[9] B. A. Malomed and A. A. Nepomnyashchii, Zh. Eksp. Teor. Fiz. **96**, 684 (1989) [Sov. Phys. JETP **69**, 388 (1989)].
[10] S. T. Milner, J. Fluid Mech. **225**, 81 (1991).
[11] M. C. Cross, P. C. Hohenberg, "Pattern Formation Outside of Equilibrium" (to be published).
[12] A. C. Newell and Y. Pomeau, "Turbulent Crystals in Macroscopic Systems" (to be published).
[13] H. W. Müller, "Model Equations for Two-Dimensional Quasipatterns" (to be published).

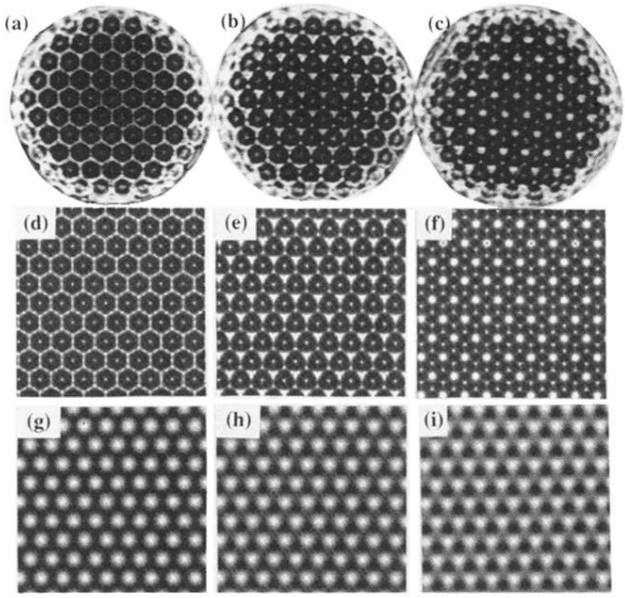

FIG. 2. Photographs (a)–(c) of nonlinear structures as observed in the T_s/H_s region of Fig. 1. For the sake of comparison computer-generated density plots are given for ideal surface patterns $\xi(x,y) = \cos(\mathbf{k}_1\cdot\mathbf{r})+\cos(\mathbf{k}_2\cdot\mathbf{r})+\cos(\mathbf{k}_3\cdot\mathbf{r}+\Phi)$, where $|\mathbf{k}_i| = k$ and $\mathbf{k}_1+\mathbf{k}_2+\mathbf{k}_3 = 0$. $\Phi = 0$ produces hexagons (g), $\Phi \simeq \pi/4$ triangles (h), and $\Phi = \pi/2$ regular triangles (i). The associated video images calculated by considering the experimental visualization technique are shown in (d)–(f).

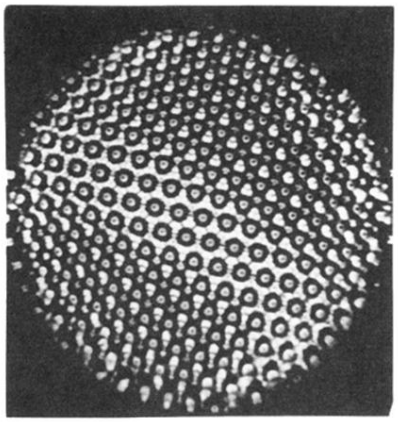

FIG. 5. Snapshot of a transient space dependent phason state. A wall of hexagons separates to areas of triangles. The picture has been taken from a cylindrical plastic container of 120 mm inner diameter with a mirror on the bottom to improve pattern visualization.